Desalination and Water Treatment
www.deswater.com
doi: 10.5004/dwt.2020.25191

182 (2020) 277–287
April

Treatment of water contaminated with diazinon by electro-Fenton process: effect of operating parameters, and artificial neural network modeling

Mohamed Gar Alalm[a,*], Mahmoud Nasr[b]

[a]*Department of Public Works Engineering, Faculty of Engineering, Mansoura University, Mansoura, 35516, Egypt, Tel. +20 12-89488300; emails: m_gar_alalm@yahoo.com/m_gar_alalm@mans.edu.eg (M.G. Alalm)*
[b]*Sanitary Engineering Department, Faculty of Engineering, Alexandria University, 21544, Alexandria, Egypt*

Received 23 April 2019; Accepted 16 November 2019

ABSTRACT

This study investigates the influence of various parameters on the performance of electro-Fenton process for degradation of diazinon. Two dimensionally stable stainless steel electrodes were used for the sake of feasibility. Optimal conditions of current intensity (*I*), pH, Fe^{2+} amount, and initial diazinon concentration were deeply studied. Complete removal of diazinon was reached after 60 min of reaction at initial concentration of 2.5 mg/L. The favored current intensity was 300 mA using 20 mg/L of Fe^{2+}. The kinetics of diazinon degradation was described by pseudo-first order pattern. In addition, an artificial neural network (ANN) model was developed to describe the relation between the operational parameters and diazinon degradation. The findings indicated that ANN provides reasonable predictive performance (R^2 = 0.994) accounting for training, validation, and test. A pure quadratic model was also developed, and implied correlation of (R^2 = 0.896) regarding the total variation of the diazinon degradation.

Keywords: Artificial neural network (ANN); Diazinon; Electro-Fenton; Stainless steel; Wastewater

1. Introduction

The growth of agro-chemical and pesticides industry has heightened the concern about the bio-recalcitrant contaminants in industrial and municipal wastewaters [1]. Industrial contaminants such as dyes, pharmaceuticals, pesticides and phenolic compounds may badly affect the aquatic, environmental systems, and public health because of their toxic and carcinogenic nature [2].

Moreover, the toxicity and non-digestibility of these compounds restrict the treatment by conventional biological methods [3]. At the present time, the development of advanced chemical-based technologies for wastewater treatment is of extreme concern for both environmental professionals and industry stakeholders [4]. In this context, many researchers have decided to study the feasibility of advanced oxidation processes (AOPs) for removal of bio-recalcitrant organics from water [5–7].

AOPs depend on the generation of hydroxyl radicals which are able to degrade persistent organic molecules until their mineralization. These radicals can be generated by physical, chemical, photo-chemical or electro-chemical methods [8]. Fenton reaction–based processes are effective and feasible treatment methods because of their fast reaction rates and the limited toxicity of Fenton reagents [9]. However, the classic Fenton reaction needs the addition of external H_2O_2, which is a powerful reactive oxidant and is dangerous to transfer and handle [10]. In addition, the conventional Fenton process produces large volume of iron sludge which needs further treatment and disposal [11]. Recently, many processes have been developed from classic Fenton reaction such as photo-Fenton, electro-Fenton, and

* Corresponding author.

Fenton-like reaction to overcome the drawbacks associated with the classic Fenton reaction [12,13]. Among these processes, electro-Fenton is considered a practical Fenton-based method, which depends on continual yielding of hydroxyl radicals by electro-produced H_2O_2 [14,15].

In electro-Fenton method, hydroxyl radicals are electrocatalytically produced in acidic solutions containing adequate amount of dissolved oxygen and ferrous ions [16]. The negative potential near the negative electrode surface leads to the reduction of dissolved oxygen to produce hydrogen peroxide [17]. The added ferrous ion reacts with the generated hydrogen peroxide to produce hydroxyl radicals and ferric ions which is considered a Fenton reaction. The formed ferric ions are reduced back to ferrous ions near the cathode surface [16,18]. Meanwhile, water is oxidized on the anode surface to generate more dissolved oxygen in the solution. This cycle provides continual production of hydroxyl radicals with less sludge amount during the electro-oxidation reaction [19]. The produced hydroxyl radicals are very strong reactive species which can be used to oxidize resistant and hazardous organics like pesticides and phenols [20].

The electro-Fenton process is typically influenced by several operational factors, viz., pH, initial contaminant concentration, Fe^{2+} dose, current intensity, etc. The effects of these variables on the degradation efficiency of contaminants can be described by regression analysis. Response surface methodology (RSM) is a multivariate method used to evolve correlations between a number of inputs and a response of interest through fitting a polynomial equation to the experimental data [21]. RSM develops a group of statistical and mathematical techniques that can be used to describe, optimize, and improve the system performance [22]. Artificial intelligence including an artificial neural network (ANN) is another technique that can be performed to determine the performance of electro-Fenton oxidation process. ANN is composed of a group of highly interconnected processing units (known as neurons) that work in parallel to model complex problems [23]. ANN has the ability to capture non-linear relationships by linking input variables with each other and with the output values [24]. The ANN model predicts the best possible response by accomplishing three steps of training, validation, and test [25]. To the best of our knowledge, there is a lack of information about the application of ANN modeling to estimate pesticides removal using electro-Fenton oxidation process.

The main objective of this work is to assess the feasibility of utilizing electro-Fenton process for treatment of pesticides contaminated wastewater. Electro-Fenton was applied on water contaminated by a pesticide, namely diazinon as a substrate. ANN was used for modeling the influence of operational conditions such as reaction time, initial concentration, current intensity (I), Fe^{2+} dose, and pH on the performance of diazinon degradation.

2. Materials and methods

2.1. Experimental

2.1.1. Materials

Diazinon (chemical formula in Fig. 1) was purchased from Merck, Germany. Acetonitrile and $FeSO_4{\cdot}7H_2O$ were purchased from Acros, Germany. All obtained chemicals were of analytical grade and used without additional treatment. HCl solution was added to contaminated water to adjust it to the desired pH.

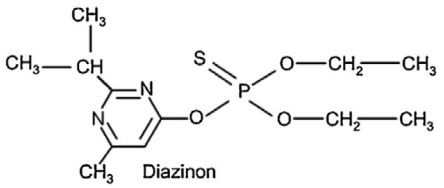

Fig. 1. Chemical structure of diazinon.

2.1.2. Experimental procedure

Experimental work was carried out at room temperature (25°C ± 3°C) with an unseparated 1,000 mL cylinder containing 650 mL of diazinon aqueous solution. Two stainless steel electrodes (5 cm × 5 cm × 0.5 cm) fixed vertically in the bottom of the vessel get uniform potential distribution. An air compressor was supplied to induce air bubbles in the water before and during the reaction. The purpose of air bubbles is to increase the dissolved oxygen which has a vital role in H_2O_2 formation. The pH was adjusted by drops of diluted HCl and a certain amount of $FeSO_4{\cdot}7h_2O$ solution was added under vigorous mixing using a magnetic stirrer. A galvano-static DC power supply was connected to the electrodes to provide and control the electrical current. A voltmeter (Digital Voltmeter [G-1002-500]), and an ammeter (PHYWE, Model No: 07038) were used to measure potential and current intensity (I), respectively.

2.1.3. Analytical methods

Diazinon was quantified by HPLC (Agilent 1200, USA) and total organic carbon (TOC) was measured by TOC analyzer (Analytik Jena, multi N/C 2100, Germany). Samples were taken periodically during the reaction and filtered by 0.2-μm syringe filters. A volume of 25 μL from each sample was injected by auto-sampler into a C18 column with a flow rate of 1.2 mL min^{-1}. The mobile phase was a mixture of 70% acetonitrile and 30% distilled water. The detection wavelength for diazinon was 254 nm.

2.2. Design of an ANN

2.2.1. Regression analysis

A pure-quadratic model (Eq. (1)) was developed to predict the degradation performance of diazinon using the input variables of pH, initial pesticide concentration, Fe^{2+} dose, current intensity, and reaction time. This model contains constant, linear, and squared terms [26]. The values of the model coefficients were computed by the method of least squares through minimizing the summed square of residuals [27]. The coefficient of determination (R^2-value) and adjusted R^2-value were used to express the model predictive accuracy. A statistics t-test was performed to determine the variables that significantly influence the diazinon removal. All calculations were carried out by computer program MATLAB R2015b.

$$Y = \beta_0 + \sum_{i=1}^{5} \beta_i x_i + \sum_{i=1}^{5} \beta_{ii} x_i^2 \quad (1)$$

where Y is the predicted diazinon removal efficiency (%), β_0 is the model intercept, β_i is the linear effect term, β_{ii} is the quadratic effect term, and x_i is the value of each independent variable; that is, pH (3–7), initial pesticide concentration (25–200 mg/L), Fe^{2+} dose (5–30 mg/L), current intensity (100–400 mA), and reaction time (10–120 min).

2.2.2. Neural network structure

An ANN model is used to predict the removal efficiency of diazinon. It is composed of an input layer, one hidden layer, and an output layer. The input layer had five neurons that received records from five experimental factors, viz., pH, initial pesticide concentration, Fe^{2+} dose, current intensity, and reaction time. The hidden and output layers contained eight and one neurons, respectively. Hence, the network architecture was expressed as 5–8–1 (Fig. 2). The transfer function in the hidden layer was hyperbolic tangent sigmoid "tansig" (Eq. (2)), which squashes the output values between –1 and +1. The pure linear "purlin" transfer function was selected in the output layer for function fitting, which gives outputs in the range of –∞ to +∞ (Eq. (3)). A trial-and-error method was used to determine the optimum numbers of hidden layers and neurons [28].

$$f(u) = \frac{2}{1+e^{-2u}} - 1 \qquad -1 \le f(u) \le 1 \quad (2)$$

$$f(u) = u \qquad -\infty < f(u) < +\infty \quad (3)$$

where u is the neuron's net input.

2.2.3. Data classification

The collected data were randomly divided into three sets [25]; that is, 60% for a training set, which is used to adjust the weights and biases of network through minimizing the mean squared error (MSE); 20% for a validation set, that is, used to terminate training before overfitting; and 20% for testing the generalization and usability of the ANN model.

2.2.4. ANN properties

This study developed a feedforward neural network with a backpropagation algorithm to train the ANN model. In this method, the training attributes are applied to the input layer using random initial weights, in which their effects are propagated through the network until an output is generated [24]. The response of the network is then compared with the target output to compute an error function, namely the network performance indicator. The error signal is transmitted backwards from the output layer to each node in the hidden layer, and the feedback algorithm adjusts (increases or decreases) the weights by some proportion to the error [23]. This process is then repeated until the corrected weights are obtained, where each node in the network receives an error signal that represents its contribution to the overall error [24]. At this point, the error function in weight space records

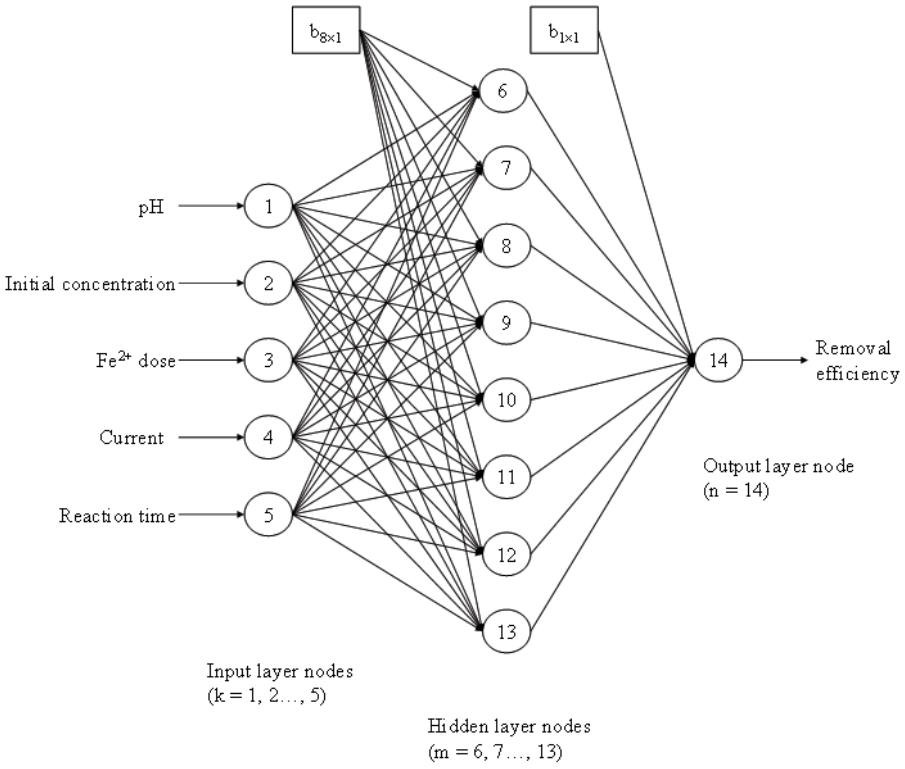

Fig. 2. Artificial neural network architecture composed of five input nodes, eight hidden nodes and one output node; that is, 5–8–1.

a minimum value corresponding to an adequate error level. In this study, Levenberg–Marquardt (trainlm) was selected as a training algorithm to update the weight values.

3. Results and discussion

3.1. Influence of initial diazinon concentration

The amount of degraded diazinon was strongly dependent on initial concentration as depicted in Fig. 3. The experimental results revealed that higher initial concentration of diazinon reduces the degradation rate, and hence additional reacting time is required for maximum diazinon removal. The removal ratios of diazinon at initial concentrations of 20, 10, and 5 mg/L were 76%, 87%, and 97%, respectively, after 90 min of reaction. At initial concentration of 2.5 mg/L, complete removal of diazinon was achieved after only 60 min of reaction. These results may be explicated by the abundance of diazinon molecules in high concentrated solutions that may require additional hydroxyl radicals to be degraded into primary and secondary by-products [20]. Moreover, hydroxyl radicals may be consumed before complete degradation of diazinon with high initial concentration, and hence additional Fenton reagent and reaction time may be required to generate sufficient amount of hydroxyl radicals [29].

The observed trend of TOC removal was different of that of diazinon as depicted in Fig. 4. The rate of TOC removal was almost time uniform and lower than diazinon degradation rate. In addition, the final removal was incomplete and less than the removal of diazinon. A TOC reduction by 62% was observed after 120 min of reaction. At the same time, the removal of diazinon was 88%, which can be attributed to formation of primary and secondary oxidation by-products during the degradation reactions [30]. Degradation of diazinon was reported to produce 2-isopropyl-6-methyl-pyrimidin-4-ol (IMP), which considered an outcome of the breakage of the P–O (pyrimi-dine group) bond [1]. IMP was reported to be a benign organic compound as compared with its origin compound diazinon [31]. Traces of diethyl 2-isopropyl-6-methylpyrimidin-4-yl phosphate (diazoxon) may be also generated during the oxidation of diazinon which causes higher levels of TOC during the reaction [1]. Moreover, additional hydroxyl radicals may be required to attain complete mineralization of the by-products, and hence the removal of TOC is slower than diazinon [32].

3.2. Influence of current intensity

Different current intensities (100–400 mA) were applied under the same operational conditions as depicted in Fig. 5. Using a current intensity of 100 and 200 mA attained a degradation efficiency of 69% and 87%, respectively, after a reaction time of 90 min. Using current of 300 mA improved the degradation of diazinon to 96.5% in 90 min and 99.5% after 120 min. At 400 mA, the diazinon degradation was accelerated at early stages of reaction, but the final degradation efficiency was not improved significantly. Consequently, 300 mA is considered the favored current intensity in this work. This finding can be demonstrated on the basis that the applied current is the engine for oxygen reduction which leads to the formation of hydrogen peroxide near the cathode surface [9]. Accordingly, increasing current intensity improves the generation of H_2O_2, and hence, Fenton reaction activity is enhanced [32].

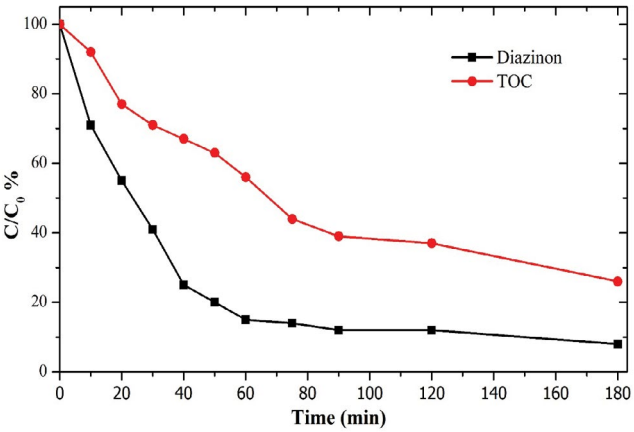

Fig. 4. Removal of TOC. Initial diazinon concentration = 10 mg/L, pH= 3.0, I = 300 mA, Fe^{2+} dose = 20 mg/L.

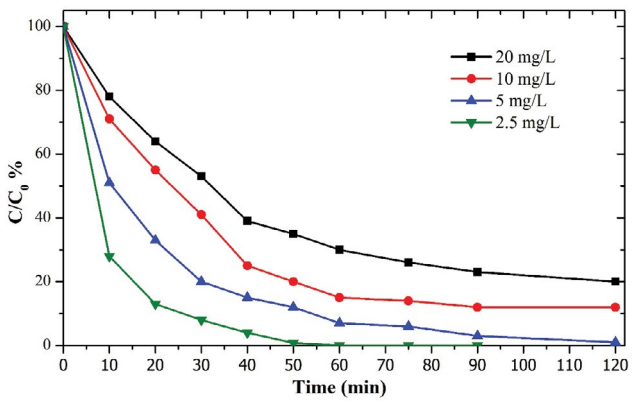

Fig. 3. Effect of initial diazinon concentration. pH = 3.0, I = 300 mA, Fe^{2+} dose = 20 mg/L.

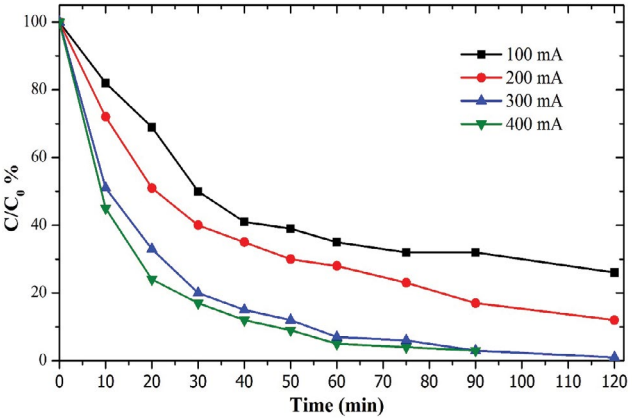

Fig. 5. Effect of current intensity. Initial diazinon concentration = 5 mg/L, pH = 3.0, Fe^{2+} dose = 20 mg/L.

3.3. Influence of pH

The degradation efficiency of diazinon under different pH is shown in Fig. 6. The results revealed that electro-Fenton process is preferable at pH ≈ 3. Increasing the pH from 3.0 to 5.0 reduced the diazinon removal rate, and hence the removal of diazinon decreased from 98% to 79% after 120 min of reaction. At neutral condition (pH ≈ 7.0), the removal rate of diazinon significantly diminished and the degradation was limited to 46% after 120 min of reaction. Similar behavior was reported for degradation of various bio-recalcitrant organic contaminants by electro-Fenton or other Fenton-based methods [12,33,34]. This finding can be explained on the fact that ferric hydroxide may be significantly produced and precipitated at pH higher than 5.0, which consumes iron species before involvement in Fenton reaction [35]. Moreover, H_2O_2 is not stable at high pH mediums and rapidly decomposes to O_2 and H_2O [9], while lower pH is favored for the production and stability of H_2O_2 [32]. On the other hand, at pH less than 3.0 hydrogen generation may be enhanced, and hence the active area for production of H_2O_2 is reduced [9,36].

3.4. Effect of Fe^{2+} dose

Fe^{2+} dose significantly influenced the degradation efficiency of diazinon as shown in Fig. 7. Using Fe^{2+} dose of 5 and 10 mg/L attained degradation of diazinon by 62% and 80%, respectively, after 120 min of reaction. Increasing the Fe^{2+} dose to 20 mg/L achieved diazinon degradation of 99%. Increasing iron amount to 30 mg/L led to enhance of degradation rates at early stages but the difference in final degradation efficiency after 120 min was not significant. Therefore, the favored Fe^{2+} dose is considered 20 mg/L. Similar trends were also reported by other researchers who investigated the degradation of bio-recalcitrant organic pollutants by electro-Fenton process [9,14,18]. The limited degradation at lower Fe^{2+} doses may be attributed to the slight formation of hydroxyl radicals due to scanty Fe^{2+} in Fenton reaction. Moreover, parasitic reactions may take place at over required Fe^{2+} doses, and consume hydroxyl radicals before the complete degradation of pollutants is attained [35].

3.5. Degradation kinetics

In order to evaluate the kinetics of diazinon degradation, the equation of pseudo-first order pattern was used. The relation between rate of degradation (r) and the concentration of diazinon (C) during the reaction time (t) are fitted to pseudo-first order kinetic equation [37].

$$r = -\frac{dC}{dt} = K_{obs}C \tag{4}$$

where k_{obs} is the constant of degradation rate. Eq. (4) can be integrated to Eq. (5) for simplification [37]:

$$\ln\left(\frac{C_0}{C}\right) = K_{obs}t \tag{5}$$

where C_0 is the initial concentration of diazinon. The experimental results of electro-Fenton process at different initial concentrations were fitted to Eq. (5). Fig. 8 depicts the linear relevance of $\ln(C_0/C)$ and reaction time at the optimum operational conditions. k_{obs} and R^2 were calculated for each case and presented in Table 1. The results showed that degradation of diazinon followed pseudo-first order model with reasonable correlation at different initial concentrations.

3.6. Statistical regression model

As listed in Table 2, a significant ($p < 0.05$) adverse effect was noticed for the linear term of x_2, indicating that the removal of diazinon could be dropped with an increase in initial concentration. Additionally, the independent variables of x_3, x_4, and x_5 had significant ($p < 0.05$) and positive linear effects on the model output. This result indicated that the degradation efficiency of diazinon could be improved with an increase in each of Fe^{2+} dose, current intensity, and reaction time. The beta coefficient associated with the quadratic term of x_2 was positive ($p < 0.05$), suggesting that the relationship between diazinon removal and initial pesticide concentration resulted in a convex curve. The squared terms of x_3, x_4, and x_5 were negative and statistically significant ($p < 0.05$),

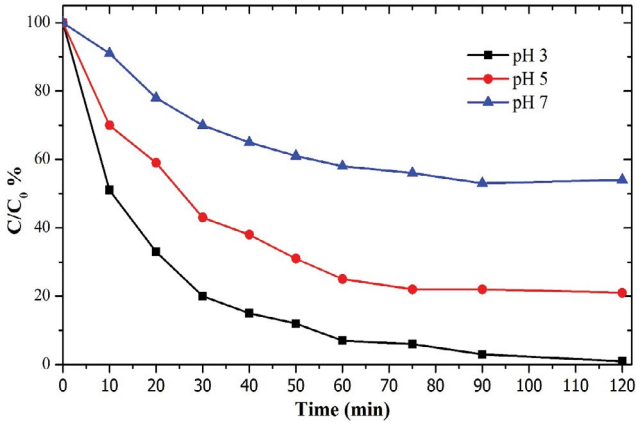

Fig. 6. Effect of pH. Initial diazinon concentration = 5 mg/L, I = 30 mA, Fe^{2+} dose = 20 mg/L.

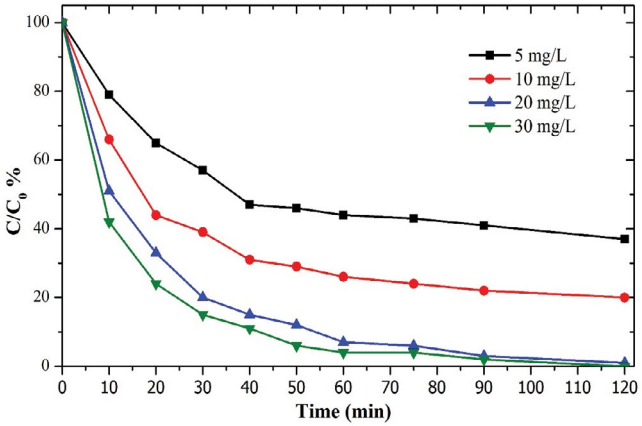

Fig. 7. Effect of Fe^{2+} dose. Initial diazinon concentration = 5 mg/L, pH = 3.0, I = 300 mA.

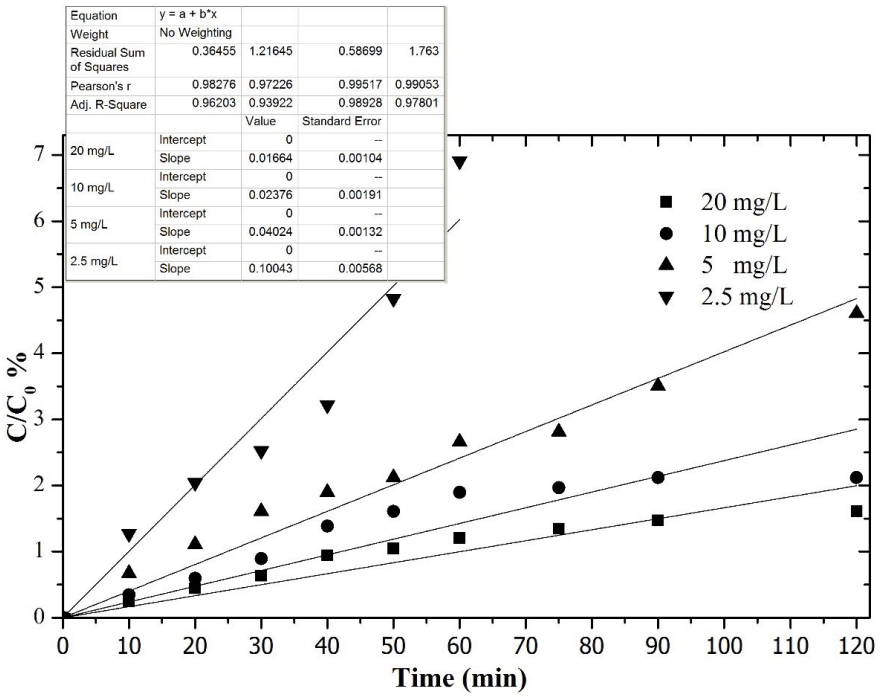

Fig. 8. Degradation kinetics of different initial diazinon concentration. pH = 3.0, I = 300 mA, Fe^{2+} dose = 20 mg/L.

Table 1
Reaction kinetics at different initial concentrations

Initial diazinon concentration (mg/L)	K_{app}	Standard error	R^2
20	0.01664	0.00104	0.96203
10	0.02376	0.00191	0.93922
5	0.04024	0.00132	0.98928
2.5	0.10043	0.00568	0.97801

indicating that the plots of diazinon removal against each of Fe^{2+} dose, current intensity, and reaction time were concave curves. However, non-significant effects ($p > 0.05$) were found for both the linear and quadratic terms of x_1: pH. Based on the aforementioned results, the effect of x_2 was quadratic linear convex down, while that for each of x_3, x_4, and x_5 was quadratic linear concave up.

The coefficient of determination (R^2-value) for the pure-quadratic model was 0.896, which implied that the model explained 89.6% of the total variation in the diazinon removal. Since the adjusted R^2-value of 0.889 was in good agreement with (close to) the R^2-value; the variables and observations of

Table 2
Diagnostic statistics representing t-test and p-values for coefficients of the pure-quadratic regression model

Variable	Regression coefficient	Std error	t Ratio	p-value	Effect[a]
	β_0: –38.8836	20.4239	–1.9038	0.0590	Non-significant
x_1	β_1: –1.4308	8.7665	–0.1632	0.8706	Non-significant
x_2	β_2: –0.4150	0.1219	–3.4039	0.0009	Significant
x_3	β_3: 3.5765	0.6006	5.9545	0.0000	Significant
x_4	β_4: 0.2535	0.0638	3.9743	0.0001	Significant
x_5	β_5: 1.7422	0.0762	22.8539	0.0000	Significant
$(x_1)^2$	β_{11}: –0.9433	0.9030	–1.0446	0.2980	Non-significant
$(x_2)^2$	β_{22}: 0.0011	0.0005	2.1219	0.0356	Significant
$(x_3)^2$	β_{33}: –0.0635	0.0174	–3.6482	0.0004	Significant
$(x_4)^2$	β_{44}: –0.0003	0.0001	–2.2685	0.0248	Significant
$(x_5)^2$	β_{55}: –0.0100	0.0006	–16.0295	0.0000	Significant

[a]Significances of variables were corrected based on p-values less than 0.05. x_1 is pH (3–7), x_2 is initial pesticide concentration (2.5–20 mg/L), x_3 is Fe^{2+} dose (5–30 mg/L), x_4 is current intensity (100–400 mA), and x_5 is reaction time (10–120 min).

the model were meaningful, and the problem of overfitting could be diminished [38].

The pure-quadratic model was used to develop an RSM that visualizes the interactive effects of independent inputs on the response. The RSM plots a 95% simultaneous confidence interval for the fitted response surface. The plot in Fig. 9 shows a contour of RSM for diazinon removal efficiency vs. the input factors of pH (3–7), initial pesticide concentration (2.5–20 mg/L), Fe^{2+} dose (5–30 mg/L), current intensity (100–400 mA), and reaction time (10–120 min). The obtained RSM can be employed to compute the diazinon removal efficiency at particular inputs. For instance (Fig. 9), at pH: 5, initial pesticide concentration: 5 mg/L, Fe^{2+} dose: 20 mg/L, current intensity: 300 mA, and reaction time: 60 min, the predicted diazinon removal efficiency was 76.42%. This value was close to the actual removal of 75% (R^2: 89.6%).

3.7. Artificial neural network

3.7.1. Training and validation performances

The plot in Fig. 10a displays the MSE performance of training, validation, and test sets against the iteration number. During training, the MSE gradually decreased along the epoch numbers until epoch 7. This pattern was satisfactory for the network training, since the purpose of training is to minimize MSE in as few epochs as possible [25]. The MSE of the validation set was monitored during the training process, in which it decreased until epoch number 1, and then initiated to increase. Hence, the iteration process was stopped at epoch 1 (i.e., MSE = 3.2742) when the MSE of the validation set begins to rise. This early stopping (even if the MSE of the training set continues to decrease) is undertaken to avoid the problem of overfitting on training data. The validation and test curves increased simultaneously after epoch 1 indicating that the training activity was discontinued before overfitting. In the case of overfitting, the training process tends to generate excess parameters that make the model more complex [26]. At this point, the model loses its generalization power resulting in reduced performance when introducing new inputs.

Fig. 10b depicts the progress of training variables concerning the magnitude of the gradient of performance and the number of validation checks. The training step is terminated if the minimum performance gradient reaches 1e-5 or if maximum validation failure becomes 6, whichever occurs first. In this study, the magnitude of the gradient (i.e., 21.751) was higher than the least error level of 1e-5, and hence the training step was stopped because the validation error failed to decrease for six iterations.

3.7.2. Optimum weights and biases

During the training phase, the weights and biases are adjusted until the network output matches the target [25]. The process of training is undertaken using a back-propagation algorithm that involves gradient descent method. Table 3 lists the connection weights ($W_{8\times5}$ and $W_{1\times8}$) and the threshold levels ($b_{8\times1}$ and $b_{1\times1}$) that provided the minimum performance function expressed as MSE on the validation set. These network parameters can be defined as follows:

Each element of the 5-length input vector ($P_{5\times1}$) was connected to each neuron in the 8-length hidden layer through 8 × 5 weight matrix ($W_{8\times5}$). The input vector was first multiplied with the weights of the connections and summed up linearly ($\Sigma W_{8\times5}\cdot P_{5\times1}$), and then 8-length bias ($b_{8\times1}$) was added; that is, $u_{8\times1} = \Sigma W_{8\times5}\cdot P_{5\times1} + b_{8\times1}$. The formed new input was transformed to the hidden layer through "tansig" activation function; that is, $f(u) = \text{tansig}(\Sigma W_{8\times5}\cdot P_{5\times1} + b_{8\times1})$. The output of this transfer function is then transmitted to the units of the following layer.

Each neuron of the 8-length hidden layer vector ($P_{8\times1}$) was connected to the single neuron in the output layer through a 1 × 8 weight matrix ($W_{1\times8}$). The outputs from the hidden units were weighted and summed up ($\Sigma W_{1\times8}\cdot P_{8\times1}$), and then a 1-length bias ($b_{1\times1}$) was added; that is, $u_{1\times1} = \Sigma W_{1\times8}\cdot P_{8\times1} + b_{1\times1}$. The resulted net input was modified by "purlin" transfer function, thereby generating an output signal; that is, $f(u) = \text{purlin}(u_{1\times1} = \Sigma W_{1\times8}.P_{8\times1} + b_{1\times1})$.

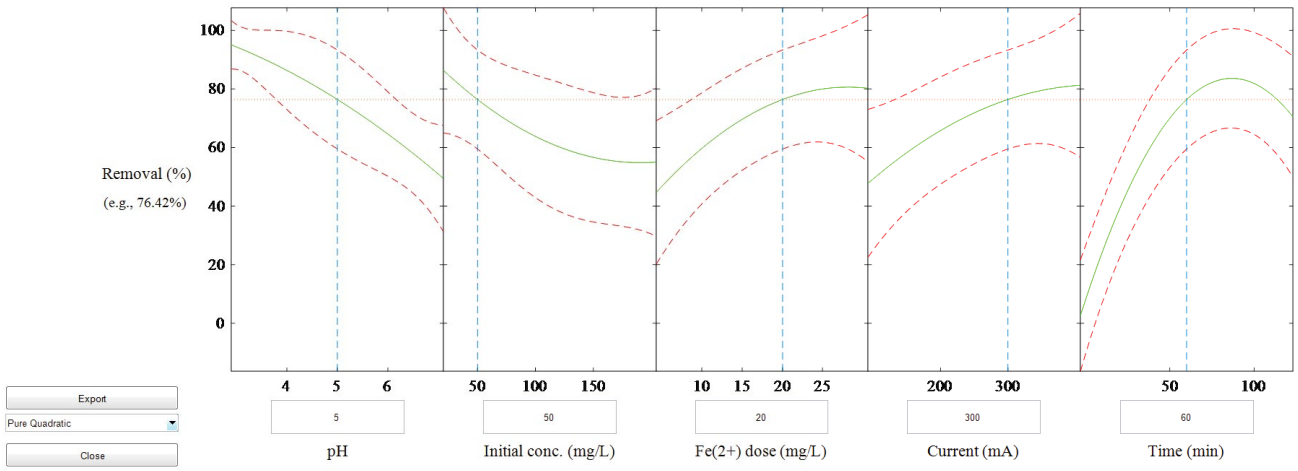

Fig. 9. Response surface plot representing the effects of pH (3–7), initial pesticide concentration (2.5–20 mg/L), Fe^{2+} dose (5–30 mg/L), current intensity (100–400 mA), and reaction time (10–120 min) on the response of removal efficiency (0–100%).

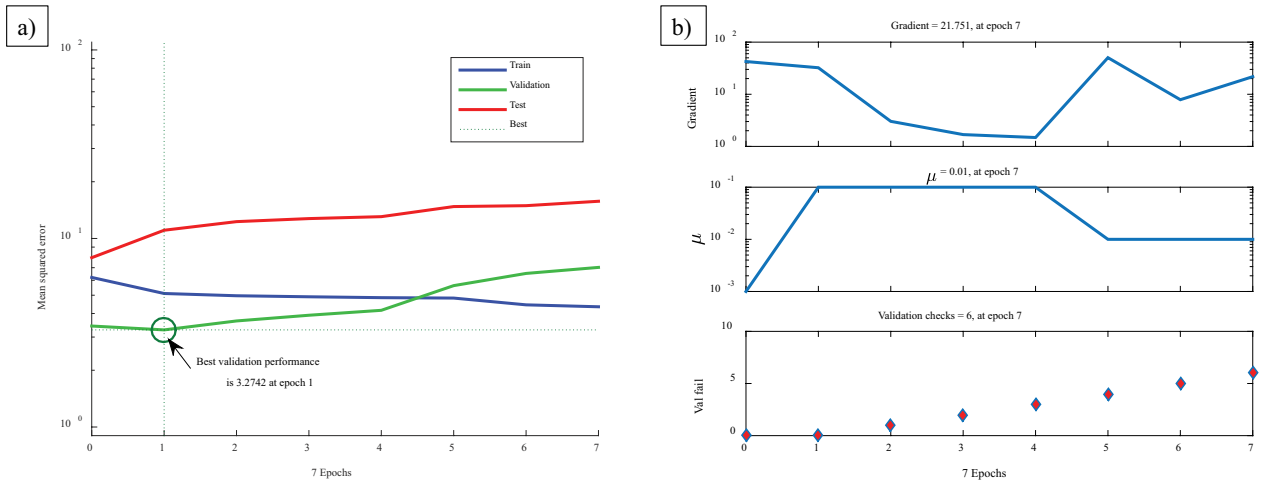

Fig. 10. ANN performance: (a) the training stopped once the MSE for validation data started to increase at epoch 1, and (b) training state gradient showing various parameters of progress.

Table 3
Weights and threshold levels of the designed ANN model

Hidden layer node	Weight from node i in input layer to node j in hidden layer for the matrix $W_{8\times5}$					Hidden layer threshold ($b_{8\times1}$)
	$k=1$	$k=2$	$k=3$	$k=4$	$k=5$	
$m=6$	0.3438	0.4583	–0.2810	–0.4645	4.9539	6.6801
$m=7$	–1.7139	–0.4300	–1.9747	–2.1332	–1.3020	1.3793
$m=8$	–0.6282	–0.5449	0.9640	0.9132	2.6195	1.2014
$m=9$	–1.8771	0.6336	–0.2817	–1.2687	–0.5808	–0.9281
$m=10$	3.1624	0.7702	0.6411	–1.1486	–1.8205	0.4091
$m=11$	–3.0007	–0.5738	–2.1483	–1.2174	1.2585	–1.4906
$m=12$	0.1154	1.8239	1.5093	–1.8998	–0.1655	–2.4032
$m=13$	–2.1298	0.6688	0.1241	–1.5945	–0.8083	–0.9463

Output layer node	Weight from node j in hidden layer to node k in output layer for the matrix $W_{1\times8}$								Output layer threshold ($b_{1\times1}$)
	$m=6$	$m=7$	$m=8$	$m=9$	$m=10$	$m=11$	$m=12$	$m=13$	
$n=14$	2.8198	0.1556	0.4543	–1.6963	–0.2847	0.2918	1.5723	1.1076	–1.6937

3.7.3. Regression plot

The regression plot in Fig. 11 shows the coefficient of determination (R^2-value) between the network response and measured target. The dashed line corresponds to the outputs that perfectly equal to targets, whereas the solid line represents the line of best fit. The training, validation, and test plots indicated a good fit with R^2-values of 0.995, 0.997, and 0.976, respectively. The overall R^2-value accounting for training, validation, and test procedures was 0.994, indicating that the model was able to explain 99.4% of the variability in the diazinon removal efficiency. It was noticed that only 0.6% of the total variation existing in the diazinon data sets were not explained by the ANN model as opposed to 10.4% of the RSM. This result revealed that the ANN model had a better predictive power than RSM, and it could be used to forecast values exactly close to the experimental response. After the training-validation-test step, the constructed ANN can be used to predict the diazinon removal using a new set of inputs (i.e., pH, initial pesticide concentration, Fe^{2+} dose, current intensity, and reaction time).

3.7.4. Sensitivity analysis

The optimum weights of the ANN model (Table 3) were used to compute the relative importance of each independent variable (i.e., pH, initial pesticide concentration, Fe^{2+} dose, current intensity, and reaction time) on the diazinon removal efficiency. For this purpose, a sensitivity analysis was carried out using Eq. (6), which is based on partitioning the network's connection weights [38]. The relative importance method was also used to find the input variable that has the most relative influence on the model response. The arrangement of data and computation of sensitivity analysis were performed as described in previous work [26].

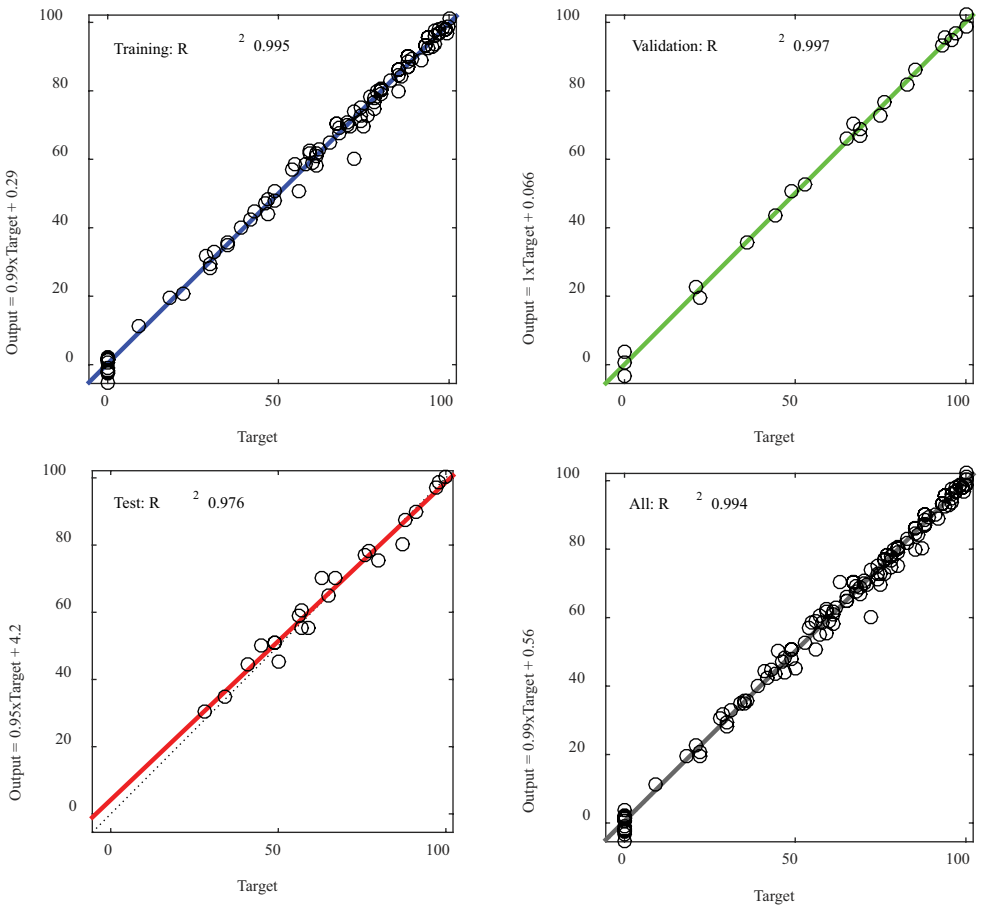

Fig. 11. Four plots showing the training, validation, testing, and overall data. The output tracks the targets very well, and the R^2-value was over 0.99 for the total response.

$$I_j = \frac{\sum_{m=1}^{m=N_h}\left(\left(\frac{\left|W_{jm}^{ih}\right|}{\sum_{k=1}^{N_i}\left|W_{km}^{ih}\right|}\right)\times\left|W_{mn}^{ho}\right|\right)}{\sum_{k=1}^{k=N_i}\left\{\sum_{m=1}^{m=N_h}\left(\left(\frac{\left|W_{km}^{ih}\right|}{\sum_{k=1}^{N_i}\left|W_{km}^{ih}\right|}\right)\times\left|W_{mn}^{ho}\right|\right)\right\}} \quad (6)$$

where I_j is the relative importance of the jth input variable on the output variable, N_i and N_h are the numbers of input and hidden neurons, respectively, W is the connection weight, the subscripts k, m, and n designate input, hidden, and output neurons, respectively, and the superscripts i, h, and o indicate input, hidden, and output layers, respectively.

The results in Fig. 12 reveal that all the input variables had strong effects on the diazinon removal efficiency. Therefore, none of the investigated variables could be excluded from this study. However, the reaction time exhibited the most important factor among the input variables with a relative index of 26%. The ranking of inputs as per relative importance was reaction time > pH > current intensity > Fe^{2+} dose > initial pesticide concentration. These results indicated that the designed network could express the behavior of the complex electro-Fenton oxidation process within the range of experimental conditions.

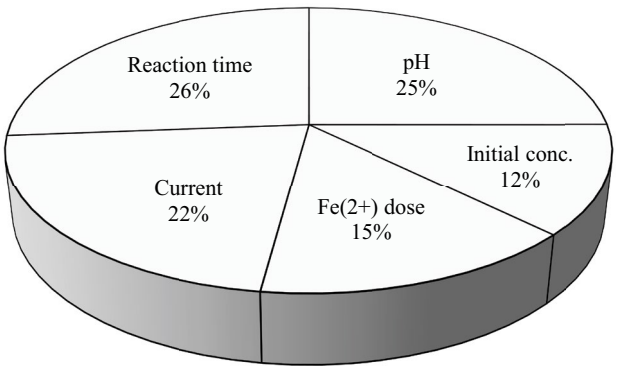

Fig. 12. Relative importance of the five input variables for the response using the ANN connection weights.

4. Conclusions

This work investigated the influence of operational conditions on the degradation of diazinon by electro-Fenton process using stainless steel electrodes. Electro-Fenton process was highly efficient at low initial diazinon concentration (2.5–5 mg/L), while at higher initial concentrations the removal of diazinon was limited to 70%. The favored

current intensity was 300 mA, and the optimal pH was 3.0. The considered dosage of Fe^{2+} was 20 mg/L. The kinetics of diazinon degradation was fitted to pseudo-first order pattern and revealed good correlation. A pure quadratic model implied that the model explained 89.6% of the total variation in the diazinon removal. The overall correlation ANN model accounting for training, validation, and test procedures was 99.4%, which means that the model could explain of the variability in the diazinon degradation efficiency.

Acknowledgment

The authors gratefully acknowledge the support from Science and Technology Development Fund (STDF) through the project No 26279.

References

[1] H. Shemer, K.G. Linden, Degradation and by-product formation of diazinon in water during UV and UV/H_2O_2 treatment, J. Hazard. Mater., 136 (2006) 553–559.
[2] R. Davarnejad, M. Mohammadi, A.F. Ismail, Petrochemical wastewater treatment by electro-Fenton process using aluminum and iron electrodes: statistical comparison, J. Water Process Eng., 3 (2014) 18–25.
[3] M. Gar Alalm, S. Ookawara, D. Fukushi, A. Sato, A. Tawfik, Improved WO_3 photocatalytic efficiency using ZrO_2 and Ru for the degradation of carbofuran and ampicillin, J. Hazard. Mater., 302 (2016) 225–231.
[4] H. Awad, M. Gar Alalm, H.K. El-Etriby, Environmental and cost life cycle assessment of different alternatives for improvement of wastewater treatment plants in developing countries, Sci. Total Environ., 660 (2019) 57–68.
[5] L. Wei, C. Shifu, Z. Wei, Z. Sujuan, Titanium dioxide mediated photocatalytic degradation of methamidophos in aqueous phase, J. Hazard. Mater., 164 (2009) 154–160.
[6] O.M. Alfano, A.E. Cassano, R.J. Brandi, M.L. Satuf, A Metho- dology for Modeling Slurry Photocatalytic Reactors for Degradation of an Organic Pollutant in Water, in: Photocatalysis and Water Purification from Fundamentals to Recent Applications, 2013, pp. 335–359.
[7] S. Navarro, J. Fenoll, N. Vela, E. Ruiz, G. Navarro, Removal of ten pesticides from leaching water at pilot plant scale by photo-Fenton treatment, Chem. Eng. J., 167 (2011) 42–49.
[8] M. Gar Alalm, M. Samy, S. Ookawara, T. Ohno, Immobilization of S-TiO_2 on reusable aluminum plates by polysiloxane for photocatalytic degradation of 2,4-dichlorophenol in water, J. Water Process Eng., 26 (2018) 329–335.
[9] P.V. Nidheesh, R. Gandhimathi, Trends in electro-Fenton process for water and wastewater treatment: an overview, Desalination, 299 (2012) 1–15.
[10] H.A. Aziz, O.M. Othman, S.S. Abu Amr, The performance of Electro-Fenton oxidation in the removal of coliform bacteria from landfill leachate, Waste Manage., 33 (2013) 396–400.
[11] Y. Wang, X. Li, L. Zhen, H. Zhang, Y. Zhang, C. Wang, Electro-Fenton treatment of concentrates generated in nanofiltration of biologically pretreated landfill leachate, J. Hazard. Mater., 229–230 (2012) 115–121.
[12] A. Babuponnusami, K. Muthukumar, Advanced oxidation of phenol: a comparison between Fenton, electro-Fenton, sono-electro-Fenton and photo-electro-Fenton processes, Chem. Eng. J., 183 (2012) 1–9.
[13] Y. Gong, J. Li, Y. Zhang, M. Zhang, X. Tian, A. Wang, Partial degradation of levofloxacin for biodegradability improvement by electro-Fenton process using an activated carbon fiber felt cathode, J. Hazard. Mater., 304 (2016) 320–328.
[14] F. Ghanbari, M. Moradi, A comparative study of electrocoagulation, electrochemical Fenton, electro-Fenton and peroxi-coagulation for decolorization of real textile wastewater: electrical energy consumption and biodegradability improvement, J. Environ. Chem. Eng., 3 (2015) 499–506.
[15] L. Labiadh, M.A. Oturan, M. Panizza, N. Ben Hamadi, S. Ammar, Complete removal of AHPS synthetic dye from water using new electro-Fenton oxidation catalyzed by natural pyrite as heterogeneous catalyst, J. Hazard. Mater., 297 (2015) 34–41.
[16] M. Gençten, A. Özcan, A detailed investigation on electro-Fenton treatment of propachlor: mineralization kinetic and degradation intermediates, Chemosphere, 136 (2015) 167–173.
[17] E. Rosales, O. Iglesias, M. Pazos, M.a. Sanromán, Decolourisation of dyes under electro-Fenton process using Fe alginate gel beads, J. Hazard. Mater., 213–214 (2012) 369–377.
[18] N. Barhoumi, L. Labiadh, M.A. Oturan, N. Oturan, A. Gadri, S. Ammar, E. Brillas, Electrochemical mineralization of the antibiotic levofloxacin by electro-Fenton-pyrite process, Chemosphere, 141 (2015) 250–257.
[19] E. Mousset, L. Frunzo, G. Esposito, E.D. van Hullebusch, N. Oturan, M.A. Oturan, A complete phenol oxidation pathway obtained during electro-Fenton treatment and validated by a kinetic model study, Appl. Catal., B, 180 (2016) 189–198.
[20] C. Annabi, F. Fourcade, I. Soutrel, F. Geneste, D. Floner, N. Bellakhal, A. Amrane, Degradation of enoxacin antibiotic by the electro-Fenton process: optimization, biodegradability improvement and degradation mechanism, J. Environ. Manage., 165 (2016) 96–105.
[21] M.A. Bezerra, R.E. Santelli, E.P. Oliveira, L.S. Villar, L.A. Escaleira, Response surface methodology (RSM) as a tool for optimization in analytical chemistry, Talanta, 76 (2008) 965–977.
[22] M. Gar Alalm, M. Nasr, S. Ookawara, Assessment of a novel spiral hydraulic flocculation/sedimentation system by CFD simulation, fuzzy inference system, and response surface methodology, Sep. Purif. Technol., 169 (2016) 137–150.
[23] M.S. Nasr, M.a E. Moustafa, H.a E. Seif, G. El Kobrosy, Application of artificial neural network (ANN) for the prediction of EL-AGAMY wastewater treatment plant performance-EGYPT, Alexandria Eng. J., 51 (2012) 37–43.
[24] R.A.T.M. Ranasinghe, M.B. Jaksa, Y.L. Kuo, F.P. Nejad, Application of artificial neural networks for predicting the impact of rolling dynamic compaction using dynamic cone penetrometer test results, J. Rock Mech. Geotech. Eng., 9 (2017) 12.
[25] A.R. Khataee, G. Dehghan, A. Ebadi, M. Zarei, M. Pourhassan, Biological treatment of a dye solution by Macroalgae *Chara* sp.: effect of operational parameters, intermediates identification and artificial neural network modeling, Bioresour. Technol., 101 (2010) 2252–2258.
[26] M. Nasr, B. Alaa El Din Mahmoud, B. Manal Fawzy, B. Ahmed Radwan, Artificial intelligence modeling of cadmium(II) biosorption using rice straw, Appl. Water Sci., 7 (2017) 823–831.
[27] H. Liu, S. Tarima, A.S. Borders, T. V Getchell, M.L. Getchell, A.J. Stromberg, Quadratic regression analysis for gene discovery and pattern recognition for non-cyclic short time-course microarray experiments, BMC Bioinf., 6 (2005) 106.
[28] M. Gar Alalm, M. Nasr, Artificial intelligence, regression model, and cost estimation for removal of chlorothalonil pesticide by activated carbon prepared from casuarina charcoal, Sustain. Environ. Res., 28 (2018) 100–101.
[29] M. Gar Alalm, A. Tawfik, S. Ookawara, Investigation of optimum conditions and costs estimation for degradation of phenol by solar photo-Fenton process, Appl. Water Sci., 7 (2014) 375–382.
[30] M. Gar Alalm, A. Tawfik, S. Ookawara, Comparison of solar TiO_2 photocatalysis and solar photo-Fenton for treatment of pesticides industry wastewater: operational conditions, kinetics, and costs, J. Water Process Eng., 8 (2015) 55–63.
[31] Y. Ku, J. Chang, S. Cheng, Effect of solution pH on the hydrolysis and photolysis of diazinon in aqueous solution, Water Air Soil Pollut., 108 (1998) 445–456.
[32] M. Gar Alalm, The Performance of Electro-Fenton Oxidation in the Removal of Pesticides from Wastewater Using Stainless Steel Electrodes, International Conference on Biology, Environment and Chemistry, Vol. 98, 2016, pp. 9–14.

[33] M. Gar Alalm, A. Tawfik, S. Ookawara, Degradation of four pharmaceuticals by solar photo-Fenton process: kinetics and costs estimation, J. Environ. Chem. Eng., 3 (2015) 46–51.
[34] A. Luis, J.I. Lombraña, F. Varona, A. Menéndez, Kinetic study and hydrogen peroxide consumption of phenolic compounds oxidation by Fenton's reagent, Korean J. Chem. Eng., 26 (2009) 48–56.
[35] E. Rosales, M. Pazos, M.a. Sanromán, Advances in the electro-Fenton process for remediation of recalcitrant organic compounds, Chem. Eng. Technol., 35 (2012) 609–617.
[36] M. Radwan, M. Gar Alalm, H. Eletriby, Optimization and modeling of electro-Fenton process for treatment of phenolic wastewater using nickel and sacrificial stainless steel anodes, J. Water Process Eng., 22 (2018) 155–162.
[37] Y.a Shaban, M.a El Sayed, A.a El Maradny, R.K. Al Farawati, M.I. Al Zobidi, Photocatalytic degradation of phenol in natural seawater using visible light active carbon modified (CM)-n-TiO_2 nanoparticles under UV light and natural sunlight illuminations, Chemosphere, 91 (2013) 307–313.
[38] A. Vijayan, G.S. Mohan, Prediction of effluent treatment plant performance in a diary industry using artificial neural network technique, Int. J. Sci. Res., 5 (2016) 2013–2016.